

JGR Atmospheres

RESEARCH ARTICLE

10.1029/2024JD041071

Key Points:

- Maximum evaporation model captured the temporal change of water surface evaporation
- The incoming and outgoing longwave radiation was coupled at a large lake
- Priestley-Taylor model with reduced Bowen ratio temperature sensitivity had the best performance

Supporting Information:

Supporting Information may be found in the online version of this article.

Correspondence to:





W. Xiao and X. Lee,
wei.xiao@nuist.edu.cn;
xuhui.lee@yale.edu

Citation:

Xiao, W., Wang, J., Zhao, R., Jia, L., Chu, H., Bao, H., et al. (2024). Evaluation of the maximum evaporation and the Priestley-Taylor models for inland waterbodies. *Journal of Geophysical Research: Atmospheres*, 129, e2024JD041071. <https://doi.org/10.1029/2024JD041071>

Received 4 MAR 2024
 Accepted 27 NOV 2024

Evaluation of the Maximum Evaporation and the Priestley-Taylor Models for Inland Waterbodies

Wei Xiao^{1,2} , Jun Wang¹, Ruonan Zhao³, Lei Jia¹, Haoran Chu¹ , Hengxin Bao¹, Chang Cao¹ , Pei Ge¹, Jian Yang¹, Mi Zhang¹, Zhen Zhang⁴, and Xuhui Lee⁵ 

¹Yale-NUIST Center on Atmospheric Environment, Key Laboratory of Ecosystem Carbon Source and Sink-China Meteorological Administration, Nanjing University of Information Science & Technology, Nanjing, China, ²Collaborative Innovation Center on Forecast and Evaluation of Meteorological Disasters, Nanjing University of Information Science & Technology, Nanjing, China, ³Hebei Provincial Institute of Meteorological Sciences, Shijiazhuang, China, ⁴Jiangning District Meteorological Bureau, Nanjing, China, ⁵School of the Environment, Yale University, New Haven, CT, USA

Abstract The Priestley-Taylor (PT) model is a classic model of potential evaporation of terrestrial and marine surfaces. It is now recognized that the Bowen ratio (β) implicit in the PT model is too sensitive to temperature. The model also requires the surface net radiation (R_n) as input even though R_n is not an independent external forcing. The maximum evaporation model (MEM) proposed by Yang and Roderick (2019, <https://doi.org/10.1002/qj.3481>) is a potential candidate for replacing the PT model. Past studies have evaluated the MEM for land ecosystems and for the global ocean. This study represents the first evaluation of the MEM for inland waterbodies. Results are based on eddy-covariance observation at a large lake and at a small fishpond. Although there were complex error structures and error compensation patterns among its intermediate variables, the MEM was able to reproduce the observed monthly ($R^2 > 0.95$) and interannual variability ($R^2 > 0.78$) in the lake latent heat flux. A key assumption of the MEM, that the incoming and outgoing longwave radiation is coupled, was a reasonable approximation at both the monthly and the annual time scale for the large lake and at the monthly time scale for the small fishpond. This assumption allows the MEM to treat R_n as an intermediate variable instead of a prescribed forcing. These results support the MEM as an alternative to the PT model at locations where R_n measurements are not available. In situations where R_n data is available, a revised PT model with reduced β temperature sensitivity is recommended.

Plain Language Summary Lakes are an important freshwater resource for the society. Accurate prediction of how much lake water is lost via evaporation will improve management of this water resource. In this study, we evaluate the performance of three models of lake evaporation including the Priestley-Taylor model, modified Priestley-Taylor model, and maximum evaporation model, using data collected at a large lake and at a small fishpond in Eastern China. We discuss the drawbacks and strengths of each and provide a guideline on model choice contingent on input data availability. We show evidence that our model parameterizations can be used for other ice-free lakes in tropical and temperate climates.

1. Introduction

The Priestley-Taylor (PT) model (Priestley & Taylor, 1972) is widely used for calculating evaporation from surfaces with unlimited water supply. Like the Penman model (Penman, 1948), it is constrained by the surface energy balance and is therefore more accurate than empirical models such as those based on the mass transfer coefficient parameterization. It is simpler to use than the Penman model because it effectively treats the aerodynamic term as a ratio of the energy term, thus avoiding parametrization of the aerodynamic resistance. Only net radiation (R_n), soil or water heat storage (G), and surface temperature (T_s) are needed as model inputs. The PT model is the preferred choice for calculating evaporation of waterbodies (e.g., Fisher et al., 2023; Han & Guo, 2023; Z. Liu et al., 2022; McMahan et al., 2016). For terrestrial surfaces with water limitation, the PT model is often used to determine the upper limit of evaporation, and the actual evaporation is obtained by adjusting this theoretical limit downward by an amount that depends on soil moisture availability (e.g., Fisher et al., 2023; Yao et al., 2015).

The simplicity of the PT model comes with two drawbacks. First, implicit in the PT model is a functional dependence of Bowen ratio β on T_s (Hicks & Hess, 1977). The accuracy of this function was first questioned by Andreas and Cash (1996) using limited data collected in snow-covered ground, lakes, and ocean surfaces. More

recently, using monthly data over the global ocean, Yang and Roderick (2019) found that the PT model overestimates β for $T_s < 297$ K and underestimates β for $T_s > 297$ K. Z. Liu and Yang (2021) confirmed a similar bias pattern with FLUNXET data collected in terrestrial ecosystems under conditions of ample soil water supply. These implicit β biases may be the reason for why the PT model underestimates the evaporation of a subtropical lake in the winter ($T_s < 280$ K; Xiao et al., 2020). Second, the requirement that R_n be a model input is problematic in two respects: (a) there is interdependence between R_n , T_s , and evaporation E . Under the same incoming solar radiation, a stronger E will result in a lower T_s , and in turn, the outgoing longwave radiation will be lower, leading to a greater R_n . In other words, R_n is not an independent external forcing variable; (b) R_n is not a standard measurement at lake surfaces, limiting the utility of the PT model.

To address these issues, Yang and Roderick (2019) developed a new theory of potential evaporation, a theory they refer to as the maximum evaporation model (MEM). In this theory, the β - T_s relationship is optimized using observations over the global ocean. If for a particular site observational data on R_n are available, the theory can be used to calculate the site evaporation, requiring R_n , T_s , and G as inputs as the original PT model. (In this study, this mode of application is referred to as the mPT model.) More generally, R_n is predicted from coupling between the incoming longwave radiation from the atmosphere (R_{li}) and the outgoing longwave radiation from the surface (R_{lo}) and from the feedback between E and T_s . The theory treats the incoming solar radiation as the true external forcing and estimates the two longwave radiation terms as intermediate variables. The calculated E has a local maximum when plotted as a function of T_s . This maximum E is regarded as the true evaporation rate of the wet surface. The theory, originally developed for the open ocean, has been shown to perform well for land ecosystems with saturated soils (Tu et al., 2022; Tu & Yang, 2022). So far, it has not been tested for inland waterbodies.

One assumption of the MEM is that R_{li} is fully coupled with R_{lo} . This assumption is not valid at short (e.g., hourly) time scales because synoptic weather variations can cause changes in R_{li} that are unrelated to R_{lo} of the local domain. But observational evidence supports its validity at the monthly time scale (Tu et al., 2022; Yang & Roderick, 2019). Currently, two open questions remain. The first one is whether this assumption holds at the annual and interannual time scales. At these time scales, R_{li} is influenced by trends in cloud cover (Raghuraman et al., 2023) and by background air temperature change and the buildup of water vapor in the atmosphere due to rising temperatures (Stephens et al., 2012). In modeling studies of evaporation trends over decades or longer, R_{li} is generally treated as an external forcing variable, not an intermediate variable coupled to the surface evaporation itself (Golub et al., 2022; Wang et al., 2018). There is a need to investigate if the MEM can accurately describe interannual variability of evaporation. The second open question concerns the coupling between R_{li} and R_{lo} of small ecosystems. It is reasonable to expect full coupling between R_{li} and R_{lo} if the underlying surface is extensive, such as the open ocean or a large lake. In the case of a small ecosystem such as a fishpond, its evaporation is only a small contributor to the pool of water vapor in the overlaying atmosphere. Currently, there are more than 11.7 million inland waterbodies with dimension smaller than 100 m in the world (Downing et al., 2006; Verpoorter et al., 2014). It is not known how well R_{li} and R_{lo} are coupled at these small spatial scales.

One goal of this study is to investigate the above two open questions, using continuous eddy covariance observations made at Lake Taihu and at a fishpond site in Eastern China. Lake Taihu is a large lake with area of 2,400 km² and is an ideal site to evaluate the coupling assumption. The fishpond is small (area 0.03 km²) and is typical of small waterbodies in Eastern China. The Lake Taihu data set spans 12 years from 2011 to 2022 and the fishpond data set spans 6 years from 2017 to 2022. The specific objectives of this study are: (a) to evaluate the PT model, the mPT model and the complete MEM for calculating water surface evaporation; (b) to evaluate the coupling assumption at the annual and interannual time scales; and (c) to compare the performance of these models for the large lake and the small fishpond.

2. Materials and Methods

2.1. Observations

Lake Taihu is the third largest freshwater lake in China. Located in the Yangtze River Delta, Eastern China, it has an area of 2,400 km² and a mean depth of 1.9 m. Lake evaporation, sensible heat flux, microclimate variables, and the four components of the radiation budget were observed at half-hourly intervals starting from the summer of 2010 and at multiple locations in a program called the Lake Taihu Eddy Flux Network (Lee et al., 2014). The present study uses the data collected at Bifenggang (site ID BFG; 31°10'N, 120°24'E), the longest running site of

the network. Fetch is greater than 4 km in all directions. Water temperature was measured at 0.20-, 0.50-, 1.00-, and 1.50-m depth. The water surface temperature was determined by the longwave radiation measurement, as

$$T_s = \sqrt[4]{\frac{R_{lo} - (1 - \epsilon) R_{li}}{\epsilon \sigma}} \quad (1)$$

where emissivity ϵ takes a dimensionless constant value of 0.97 for waterbodies (Campbell & Norman, 2012) and σ is the Stephan-Boltzmann constant. The albedo of this site was 0.079. Details regarding instrumentation, data quality control, and gap-filling procedures are given by Xiao et al. (2020) and Z. Zhang et al. (2020). According to the 0.20-m depth water temperature record, the lake was not frozen except for short periods from 23 to 27 January 2016 and for several hours on 31 January 2016 and 27 January 2018.

The fishpond site (31°58'N, 118°15'E) is also located in the Yangtze River Delta, with a linear distance of 200 km from Lake Taihu. The site consists of four ponds next to one another, each about the size of 110 m by 60 m. The measurement protocol was similar to that deployed at Lake Taihu. It consisted of eddy covariance measurement of lake evaporation and sensible heat flux, measurement of the four components of net radiation, and measurement of supporting microclimate variables (J. Zhao et al., 2019, 2021). The eddy covariance system was installed at the midpoint of the four ponds. The observation started from 1 June 2017 and continued to 31 December 2022. Data were reported at 30 min intervals. Data gaps were filled with the method described by Z. Zhang et al. (2020). Water temperature was measured at 0.20-, 0.50-, and 0.80-m depth. The water surface temperature was determined with Equation 1. The fishpond albedo was 0.041. According to the record of 0.20-m water temperature, there was no ice during the whole period except for the nights between 10 and 12 February 2018, lasting 4–7 hr in each night.

2.2. Evaporation Models

2.2.1. The Priestley-Taylor (PT) Model

The PT model expresses the latent heat flux λE as

$$\lambda E = 1.26 \frac{\Delta}{\Delta + \gamma} (R_n - G) \quad (2)$$

where Δ is the slope of the saturated vapor pressure versus temperature relationship (evaluated at T_s) and γ is the psychrometric constant. This equation implies the following relationship between β and T_s ,

$$\beta = 0.79 \gamma / \Delta - 0.21 \quad (3)$$

(Hicks & Hess, 1977).

2.2.2. The Modified Priestley-Taylor (mPT) Model

Yang and Roderick (2019) show that the β - T_s relationship described by Equation 3 is not accurate. A more accurate expression, calibrated against the monthly ocean surface heat fluxes and the sea-surface temperature data in the global ocean surface evaporation product (Version 3) from the Objectively Analyzed Air-sea Flux (OAFflux) project (Yu & Weller, 2007), is

$$\beta = 0.24 \gamma / \Delta \quad (4)$$

The surface energy balance equation is

$$\lambda E + H = R_n - G \quad (5)$$

Noting that $\beta = H/\lambda E$ and making use of Equation 4, we obtain from Equation 5 the modified PT model (mPT model)

$$\lambda E = \frac{\Delta}{\Delta + \eta\gamma}(R_n - G) \quad (6)$$

where the coefficient η is 0.24 for the open ocean.

2.2.3. The Maximum Evaporation Model (MEM)

Both the PT and the mPT model require that R_n and T_s be known. The MEM bypasses this requirement by treating R_n and T_s as implicit variables. A brief description of the MEM is given below for the reader's convenience.

In the MEM, albedo (α) is a prescribed parameter, and the incoming solar radiation R_{si} is an external forcing variable provided by field observation. The net radiation is given as

$$R_n = R_{si} - R_{so} + R_{li} - R_{lo} \quad (7)$$

where the outgoing shortwave (solar) radiation is given by

$$R_{so} = \alpha R_{si} \quad (8)$$

The incoming longwave radiation R_{li} is given by

$$R_{li} = \sigma(T_s - \Delta T)^4 \quad (9)$$

Equation 9 indicates that the effective blackbody radiative temperature of the atmosphere is lower than the surface temperature by ΔT . In the MEM, this temperature difference ΔT is parameterized as a function of latitude (lat) and atmospheric transmissivity (τ), the latter of which is calculated as the ratio of the observed monthly incoming solar radiation at the surface to that at the top of the atmosphere. The parameterization for ΔT is given by

$$\Delta T = 2.517 \exp(2.38\tau) + 0.03466|lat| \quad (10)$$

where the parameter values were obtained by Yang and Roderick (2019) using monthly incoming and outgoing shortwave and longwave radiative fluxes at the Earth's surface and the top of atmosphere over the global ocean, with a spatial resolution of $1^\circ \times 1^\circ$.

The outgoing longwave radiation R_{lo} consists of radiation emitted by the surface and a small portion of R_{li} reflected by the surface (Lee, 2023; Yang & Roderick, 2019), and is calculated as

$$R_{lo} = (1 - \varepsilon)R_{li} + \varepsilon\sigma T_s^4 \quad (11)$$

In Equations 6–11, R_{si} and G are provided by observation. The two unknowns are λE and T_s . They are obtained numerically by finding the local maximum of λE in relation to T_s . The numerical procedure consists of four steps: (a) setting up a loop for T_s in the range from 0°C to 40°C with an interval of 0.01°C ; (b) calculating λE using the above set of the equations at each interval of T_s ; (c) plotting λE as a function T_s ; and (d) finding the maximum λE . The maximum λE and the corresponding T_s are taken as the true latent heat flux and the estimated water surface temperature.

If the local observations at Lake Taihu were used to optimize the ΔT parameterization, Equation 10 was changed slightly to

$$\Delta T = 2.175 \exp(2.7056\tau) + 0.0664|lat| \quad (12)$$

The MEM calculation of λE was performed at both the monthly and the annual scale, using monthly or annual mean radiation and meteorological inputs.

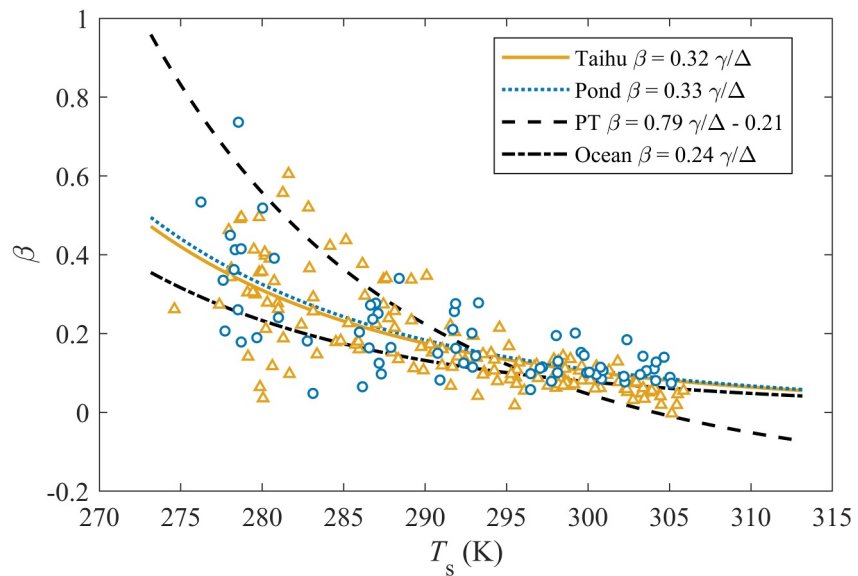


Figure 1. The relationship between monthly Bowen ratio and surface temperature according to observations at Lake Taihu (triangles) and the fishpond (circles), the Priestley-Taylor (PT) model, and the global ocean observation.

3. Results

3.1. Relationship Between Bowen Ratio and Temperature

We found that the η value of 0.24 causes underestimation of the Bowen ratio at Lake Taihu and at the fishpond site. Tuning against the observed monthly β and T_s , we obtained $\eta = 0.32$ for Lake Taihu and $\eta = 0.33$ for the fishpond site (Figure 1). Using a shorter data set we published earlier, Z. Liu and Yang (2021) obtained the same η value for the lake site. In the following, we adopt these local values for evaluating the performance of the mPT model and the MEM.

The data presented in Figure 1 are monthly values. At the annual time scale, a larger PT coefficient has been reported (Han & Guo, 2023; Xiao et al., 2020). However, we are unable to establish an annual relationship between β and T_s due to the small range of the annual T_s (less than 2.2°C). In the following, model calculations were carried out at the monthly time step.

3.2. Model Performance

Generally, all the three models are able to reproduce the observed seasonal variations in λE , with lower values in the winter and higher values in the summer (Figure 2). At the monthly time scale, the modeled λE explains over 95% of the observed λE across the three models and the two sites (Table 1). The seasonal composite plot reveals that the PT model has a high bias in the summer season and a low bias in the winter season (Figures 3a and 3d). The mean biases are +6.1 and +13.6 W m^{-2} in August and -4.5 and -6.0 W m^{-2} in January for Lake Taihu and the fishpond, respectively. These biases result from the inaccurate β - T_s relationship implicit in the PT model (Equation 3). The use of locally tuned β - T_s relationship in the mPT model makes these biases disappear (Figures 3b and 3e). The MEM has seasonal biases in an opposite phase to the PT model, showing a mean bias of -20.8 and -8.3 W m^{-2} in August and +12.2 and +6.2 W m^{-2} in January for Lake Taihu and the fishpond, respectively. The high biases and opposite signs in August and January indicate overestimation of R_{in} in the winter and underestimation of R_{in} in the summer.

During the 12-year observational period at Lake Taihu (Figure 4a), the annual averaged λE shows a generally increasing trend, from the lowest value of 76.1 W m^{-2} in 2011 to the highest value of 92.2 W m^{-2} in 2022. The three models have reproduced the trend and interannual variability reasonably well (Figure 4c). The coefficient of variation R^2 ranges from 0.78 (MEM, Lake Taihu) to 0.88 (mPT, Lake Taihu, Table 1). The PT model was biased low, with ME of -6.4 W m^{-2} and root mean square error (RMSE) of 6.8 W m^{-2} . The mPT simulation was closer

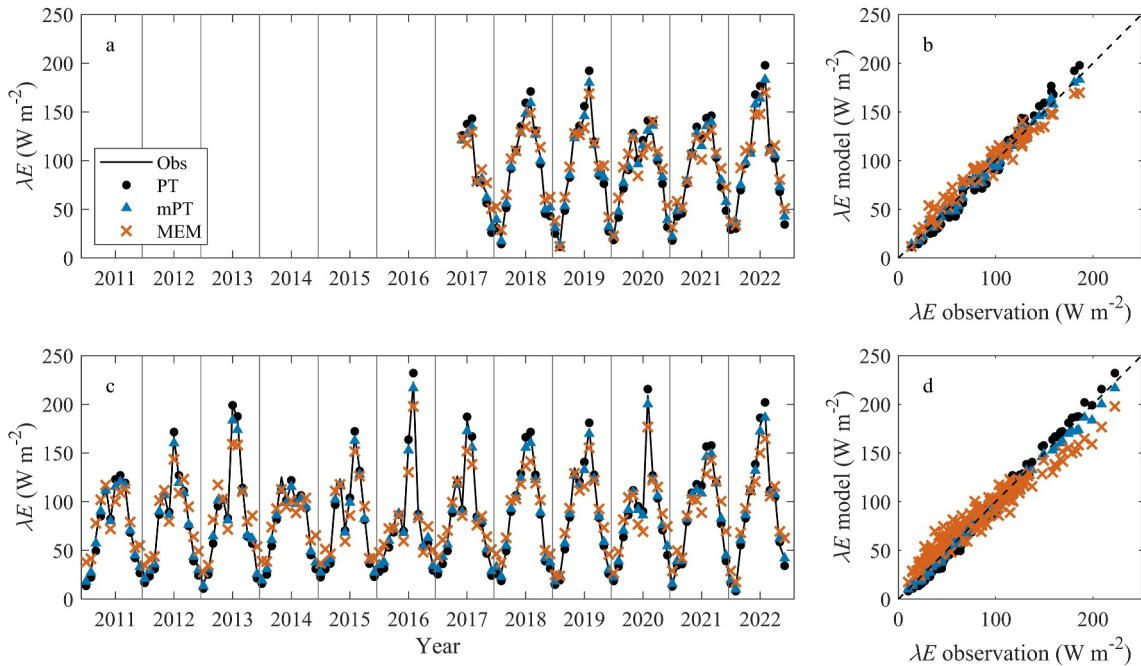


Figure 2. Comparison of observed monthly latent heat flux with predictions by the Priestley-Taylor (PT), the modified Priestley-Taylor (mPT), and the maximum evaporation model (MEM) for the fishpond (a, b) and for Lake Taihu (c, d).

to the observation, with ME of $-3.2 W m^{-2}$ and RMSE of $3.7 W m^{-2}$. The MEM simulation had the best agreement with the observation, with ME of $1.5 W m^{-2}$ and RMSE of $2.7 W m^{-2}$.

3.3. Comparison Between the Lake and the Fishpond

At the annual time scale, the mPT model reduces the mean error (ME) for both the lake and the fishpond by about $3.0 W m^{-2}$ and reduces the RMSE also by about $3.0 W m^{-2}$, in comparison to the PT model (Table 1). At the monthly time scale, the change in ME from PT to mPT is similar between the two sites. The MEM shows a positive ME at both sites and at both the monthly and the annual time scale, but the difference in ME between the lake and the fishpond is reversed between the two time scales: The monthly ME is greater for the fishpond and the annual ME is greater for Lake Taihu. Comparison at annual scale is inconclusive due to short annual time series for the fishpond site.

3.4. Error Compensation Among Intermediate Variables in MEM

Examination of intermediate variables of the MEM reveals complex error structures and error compensation patterns. A key intermediate variable is the surface temperature; it is used to calculate the outgoing longwave radiation R_{lo} (Equation 11), the incoming longwave radiation R_{li} (Equation 9) and the slope of the saturation vapor pressure curve Δ . At Lake Taihu, the observed monthly T_s was low in the winter and high in the summer, the

Table 1
Determination Coefficient (R^2), Mean Bias Error (ME, $W m^{-2}$) and Root Mean Square Error (RMSE, $W m^{-2}$) of Latent Heat Flux for the Priestley-Taylor (PT), the Modified Priestley-Taylor (mPT), and Maximum Evaporation Model (MEM)

Time scale	Water bodies	PT			mPT			MEM		
		R^2	ME	RMSE	R^2	ME	RMSE	R^2	ME	RMSE
Monthly	Lake Taihu	0.99	-2.1	5.6	0.99	-1.8	4.5	0.95	1.4	14.6
	Pond	0.98	-0.3	8.4	0.99	-0.4	4.5	0.96	2.4	9.7
Annual	Lake Taihu	0.85	-6.4	6.8	0.88	-3.2	3.7	0.78	1.5	2.7
	Pond	0.83	-6.3	6.5	0.85	-3.4	3.7	0.85	0.2	1.5

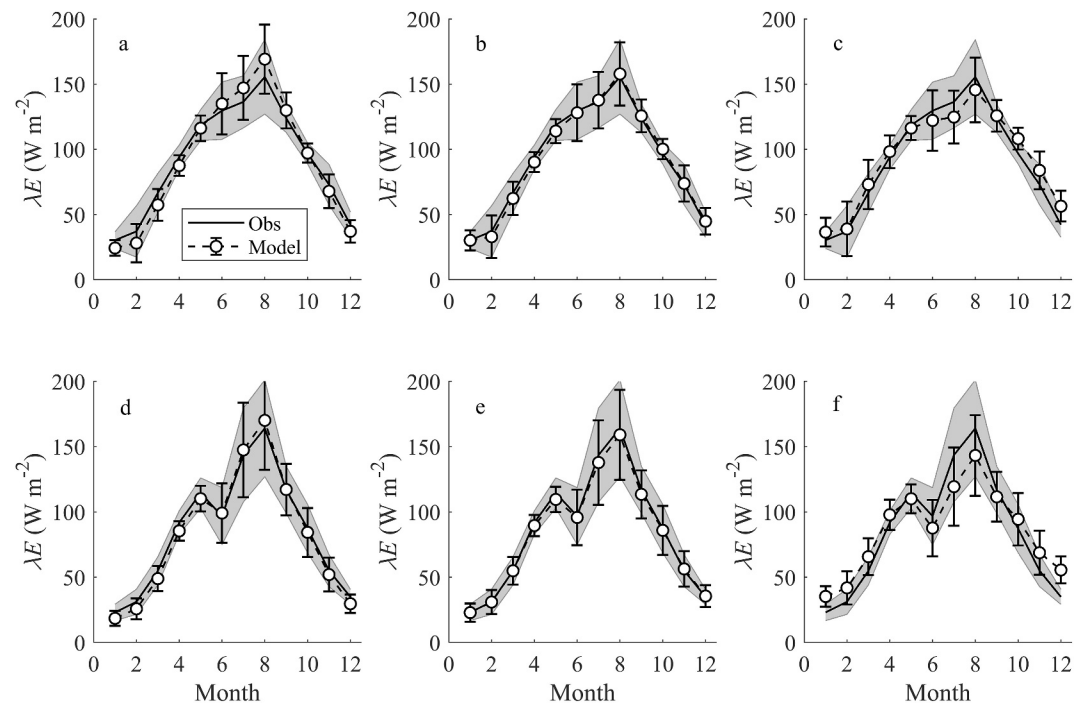


Figure 3. Seasonal composites of observed and predicted latent heat flux for the fishpond (a–c) and for Lake Taihu (d–f). (a, d): Observation and Priestley-Taylor (PT) model; (b, e): Observation and modified Priestley-Taylor (mPT) model; (c, f): Observation and maximum evaporation model (MEM).

monthly mean T_s ranging from 1.4 to 32.7°C (Figure 5). The MEM predicts a similar T_s seasonal trend ($R^2 = 0.73$), but it overestimates T_s . The mean bias in T_s is smaller in the summer (+1.0°C) than in the winter (+10.8°C). Similar biases are detected for the fishpond. This error structure is broadly consistent with Yang and

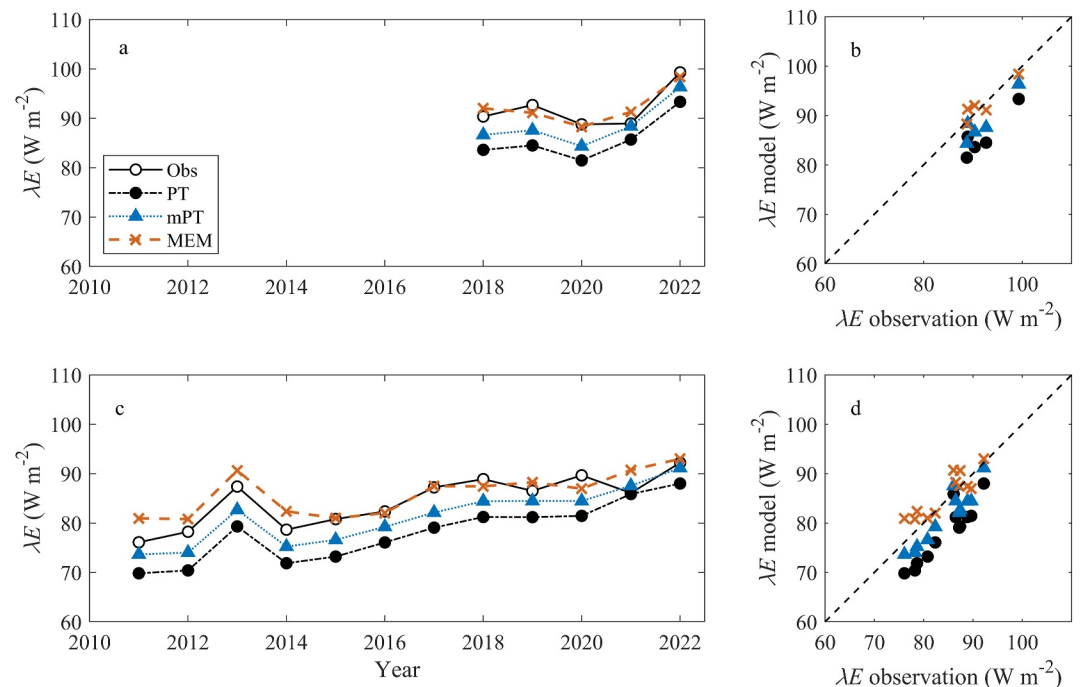


Figure 4. Same as Figure 2 but for annual latent heat flux.

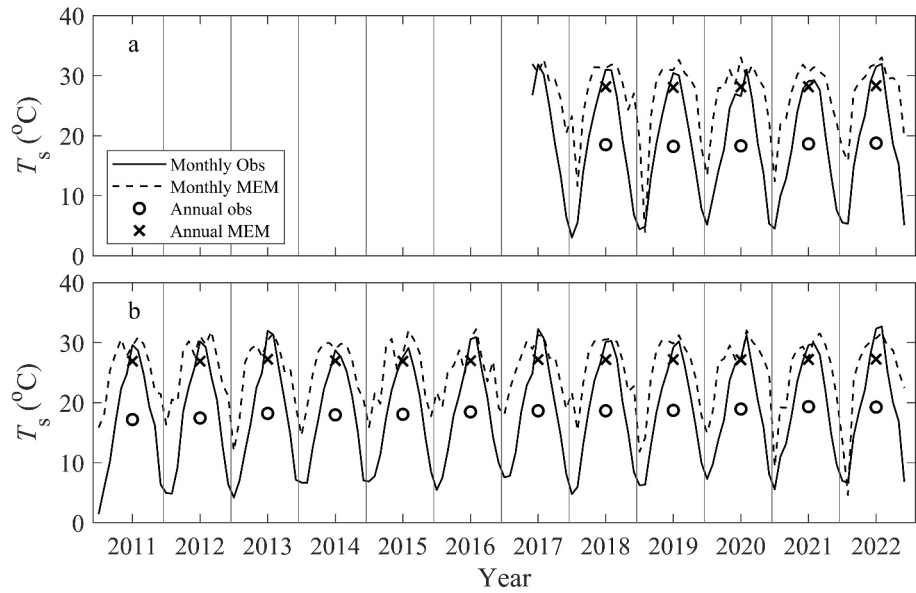


Figure 5. Time series of observed and modeled monthly and annual T_s for the fishpond (a) and for Lake Taihu (b).

Roderick (2019) who showed that the MEM T_s bias increases with decreasing temperature for the global ocean, changing from $+0^\circ\text{C}$ at an ocean surface temperature $T_s = \sim 27^\circ\text{C}$ to $+10^\circ\text{C}$ at $T_s = \sim 2^\circ\text{C}$.

Another intermediate variable is the net longwave radiation $R_{\text{in}} = R_{\text{li}} - R_{\text{lo}}$. In the MEM, this term is primarily controlled by ΔT , the difference between the surface temperature and the blackbody radiative temperature of the atmosphere, which is parameterized a function of atmospheric transmissivity τ for a given site at a fixed latitude. According to this parameterization, R_{in} is linearly dependent on τ , becoming more negative as τ increases (Figure 6). Even though the original parameterization has been optimized over a large latitudinal range across the global ocean, it captures reasonably well the temporal dependence of R_{in} on τ at our sites. In fact, use of the local ΔT parameterization (Equation 12) instead of the original parameterization (Equation 10) does not bring improvement to the monthly and annual MEM results (Figure S1 in Supporting Information S1). However, two small shortcomings deserve attention. First, when examined individually, the two longwave components show systematic biases. On the annual basis, the outgoing component is biased high by about 50 W m^{-2} which is consistent with the high bias of the modeled T_s , and the incoming component is also biased high by a similar amount (Figures 7c–7f). These two biases offset each other, resulting in much more accurate annual R_{in} than the two components (Figures 7g and 7h). Second, the model underestimates R_{in} in the summer and overestimates R_{in} in the winter (Figures 6a and 6b). The mean R_{in} bias is $+8.4$ and $+0.3 \text{ W m}^{-2}$ in January and -14.5 and -13.6 W m^{-2} in August for Lake Taihu and the fishpond, respectively.

The accuracy of the MEM λE is degraded by the bias error of T_s through its influence on the slope of the saturation vapor pressure curve Δ . This error is more serious in the winter than in the summer. The observed and modeled mean T_s are 5.7 and 15.4°C in January, respectively, for Lake Taihu (Figure 5). The corresponding Δ values are 63.5 and 112.3 Pa K^{-1} . Putting these values in Equation 6, we obtain 0.748 and 0.839 for the parameter group $\Delta/(\Delta + \eta\gamma)$. The modeled $\Delta/(\Delta + \eta\gamma)$ value is 12.1% greater than the observation, with a mean bias error of 0.0907 . The observed and modeled T_s are 30.2 and 31.1°C in August for Lake Taihu. The corresponding $\Delta/(\Delta + \eta\gamma)$ values are 0.920 and 0.923 , differing by only 0.4% , with a mean bias error of 0.0033 .

Let δ_1 denote the mean bias error in $\Delta/(\Delta + \eta\gamma)$ caused by the T_s error, and δ_2 the bias error in R_{in} . The total error in λE can be written as

$$\delta = \delta_1 \times (R_{\text{in}} - G) + \delta_2 \times \frac{\Delta}{\Delta + \eta\gamma} \quad (13)$$

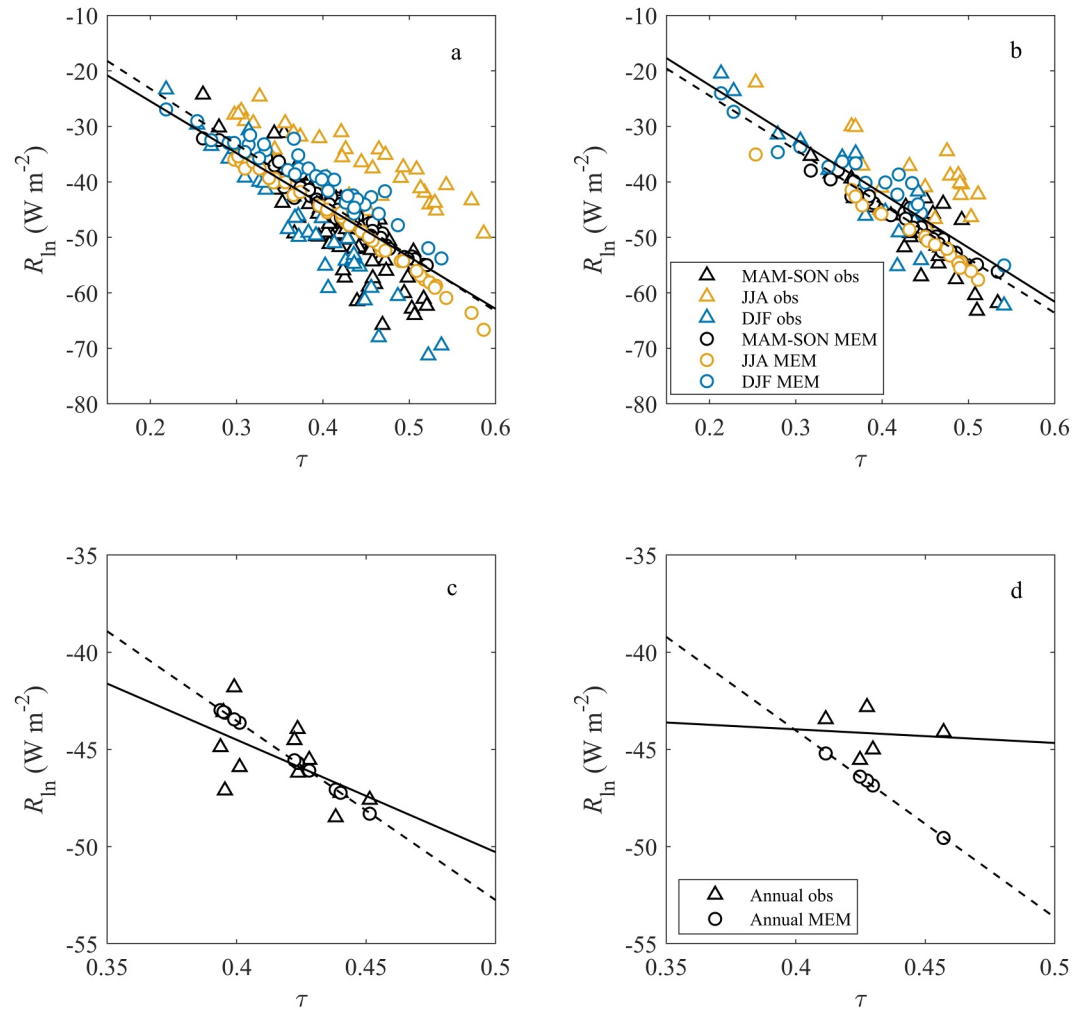


Figure 6. Dependence of observed and modeled net longwave radiation on atmospheric transmissivity for Lake Taihu (a, c) and the fishpond (b, d) at monthly (upper panels) and annual (lower panels) time scales. Data are separated by season. MAM: March, April & May; SON: September, October & November; JJA: June, July & August; DJF: December, January & February. Solid lines: regression lines for observational data; dashed lines: regression lines for model data.

Using the above bias values, δ_1 was 0.0907 and 0.0033, and δ_2 was 8.4 and -14.4 W m^{-2} in January and August, respectively. With $R_n - G$ of 42.0 W m^{-2} in January, the first and second term of Equation 13 become $+3.8$ and $+7.1 \text{ W m}^{-2}$, respectively, in January for Lake Taihu, giving a total estimated error of $+10.9 \text{ W m}^{-2}$ in λE . This estimate is good agreement of the actual bias error of $+12.2 \text{ W m}^{-2}$ (Figure 3f). In other words, the temperature error contributes 35% to the error in λE . The error partitions are $+0.5 \text{ W m}^{-2}$ (first term) and -13.4 W m^{-2} (second term) in August for Lake Taihu, indicating the λE error is dominated by the error of the net longwave radiation.

3.5. Longwave Radiation Coupling in MEM

One important assumption made by the MEM is that the outgoing and incoming longwave radiation are coupled and the difference between them is mainly dependent on atmospheric transmissivity. The coupling assumption does not hold at short time scales, such as during cold front events when lake evaporation exhibits pulse-like patterns unrelated to radiation energy input (H. Liu et al., 2011; McGloin et al., 2015). The results of Yang and Roderick (2019) and Tu et al. (2022) support this assumption at the monthly time scale. The Yang and Roderick parameterization of the longwave dependence on atmospheric transmissivity is developed primarily based on spatial correlation between the net longwave radiation and atmospheric transmissivity across the global ocean. One question is whether this relationship based on spatial variability also works for temporal variability. In

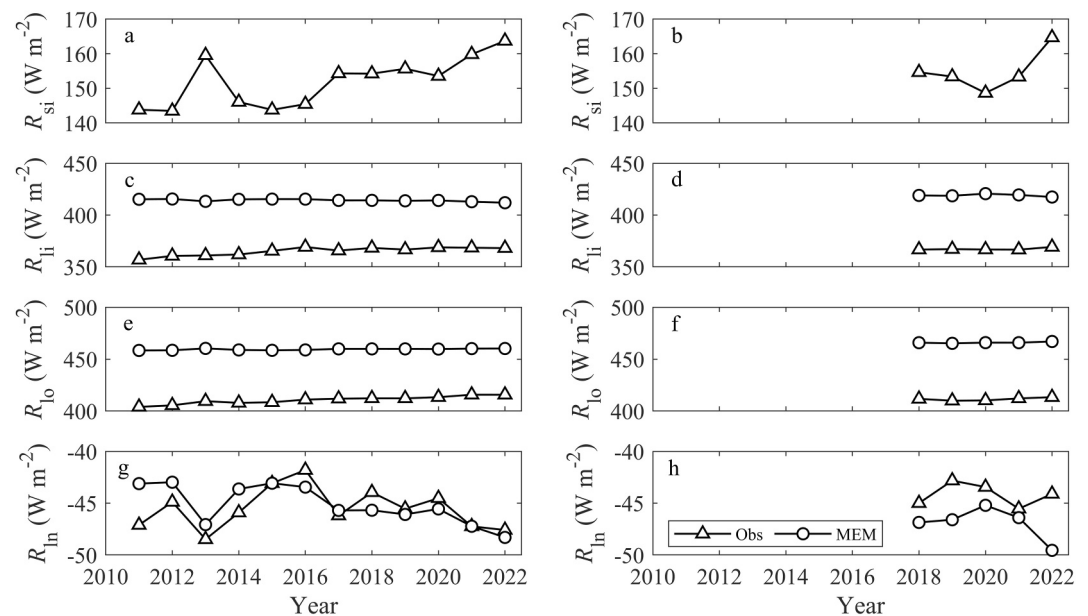


Figure 7. Time series of observed and modeled annual mean radiation components. (a, b): Incoming shortwave radiation; (c, d): Incoming longwave radiation; (e, f): Outgoing longwave radiation; (g, h): Net longwave radiation. Left panels: Lake Taihu; Right panels: fishpond.

this study, the monthly transmissivity at Lake Taihu ranges from 0.22 to 0.59, with a mean value of 0.41, and that at the fishpond ranges from 0.21 to 0.54, with a mean value of 0.42. These variations are temporal in nature, consisting of seasonal changes as well as interannual variations. The modeled R_{in} is negatively correlated with τ ($r = -0.95, p < 0.001$ for Lake Taihu; $r = -0.95, p < 0.001$ for the fishpond; Figures 6a and 6b). The observation also shows significant negative correlation ($r = -0.63, p < 0.001$ for Lake Taihu; $r = -0.75, p < 0.001$ for the fishpond; Figures 6a and 6b). These results indicate that R_{li} and R_{in} are indeed coupled at the monthly time scale at both sites.

At the annual time scale, the MEM predicts a nearly perfect correlation between R_{in} and τ (Figures 6c and 6d). The observed annual R_{in} at Lake Taihu is also correlated with τ ($r = -0.59, p < 0.05$), although the correlation is not as strong as the theoretical prediction. The dependence of the annual R_{in} on the annual transmissivity is especially evident in 2013. There was a dramatic increase of the annual incoming shortwave radiation in 2013 in comparison to the previous year (Figure 7a), indicating high transmissivity in 2013. In response, both the observed and modeled R_{in} is lower in 2013 than in 2012. The regression slope of the observed R_{in} versus τ is $-57.8 \pm 55.7 \text{ W m}^{-2}$ per unit transmissivity change (mean \pm 95% confidence bound), compared to the theoretical slope of $-92.1 \pm 0.7 \text{ W m}^{-2}$. These two slope values are not statistically different ($p = 0.129$), implying that the coupling assumption for Lake Taihu seems acceptable at the annual time scale. The results for the fishpond site are inconclusive because the annual time series for the fishpond site is too short.

The coupling assumption implies that the incoming longwave radiation of the atmosphere is regulated by the energy processes in a local domain. This seems at odds with the belief that at the annual and longer time scales, R_{li} is driven by atmospheric changes at scales much larger than the local domain and hence should be viewed as an external forcing variable, much like the incoming solar radiation (R_{si}). On the decadal time scale, there is an increasing trend in R_{li} globally. About half of this trend is contributed by rising atmospheric temperature and the other half by water vapor buildup in the atmosphere (Stephens & Hu, 2010). According to atmospheric reanalysis, R_{li} increases by 7.5 W m^{-2} for every 1 K increase in temperature (Wang et al., 2021). At Lake Taihu, R_{li} increased steadily over the 12-year observational period (Figure 7c). Xiao et al. (2020) reported that the annual R_{li} at Lake Taihu is positively correlated with water vapor pressure and cloud cover. Their attribution analysis indicates that the R_{li} change is responsible for about half of the observed interannual variations in λE . We argue that the fact that R_{li} is an external variable at these long time scales does not contradict the coupling assumption. Although interannual changes in R_{li} reflect changes in atmospheric background, these changes will induce changes in the

local outgoing longwave radiation. Perhaps at the monthly time scale, the coupling is the result of τ response to local R_{lo} (Yang & Roderick, 2019), indicating the modification of atmospheric water vapor by local processes. At the annual time scale, the coupling can be viewed mostly as the response of the local R_{lo} to τ change.

A surprising result is that the MEM performed better in two respects for the small fishpond than for the large lake. The annual mean bias in λE for the fishpond (+0.2 W m⁻²) is smaller in magnitude than for Lake Taihu (+1.5 W m⁻²). The modeled λE seasonality is in better agreement with the observed seasonality at the fishpond (Figure 3c) than at Lake Taihu (Figure 3f). In the Introduction, we ask the question about whether the coupling assumption is valid for the fishpond because its evaporation should have negligible influence on the atmospheric transmissivity. The observation data in Figure 6b imply that the monthly R_n , T_s , and λE are interdependent at the fishpond, with significant R_n - τ correlation within seasons. This interdependence is captured by the same parameterization of R_{in} versus τ in the MEM. In this regard, the coupling assumption seems a good approximation at the monthly time scale for the fishpond. At this small spatial scale, the incoming longwave radiation should be viewed as an external variable rather than a response variable. However, its seasonal variation will cause the outgoing longwave radiation of the fishpond to respond. In this interpretation, the interaction between this atmospheric forcing and the response of this small waterbody also depends on atmospheric transmissivity in the same way as the coupling between the incoming and the outgoing longwave radiation at the large lake.

4. Discussion

Our results reveal strengths and weaknesses of each of the three models of lake evaporation. One drawback of the original PT model is that its Bowen ratio is too sensitive to temperature. The PT Bowen ratio is biased high in low temperatures and biased low in high temperatures (Figure 1). For this reason, the modeled λE has a high bias in the summer season and a low bias in the winter season (Figure 3). Another drawback is that it requires R_n as an input. However, R_n is not a common measurement at lake sites.

The MEM offers a simple alternative to the PT model for locations where no R_n and surface temperature measurements are available. The only required input variables are monthly incoming solar radiation and water heat storage. Aside from this practical advantage, the MEM is considered to be more valid theoretically than the PT model or the Penman model for determining the true potential evaporation or the true atmospheric demand for evaporation of terrestrial surfaces (Tu & Yang, 2022). At our sites, the annual mean bias of the modeled λE is less than 2 W m⁻², although biases in the monthly λE are larger. Our analysis reveals complex compensation of errors between warm and cold seasons and among the model intermediate variables (surface temperature and the incoming and outgoing longwave radiation fluxes). These seasonal differences may have been caused by different cloud patterns in the winter and in the summer. The idea about longwave coupling takes into account that τ is greater if there is less water vapor in the atmospheric column, but it omits the dependence of τ on cloud patterns. Even though water vapor and cloud amount are generally correlated, the downward longwave radiation also depends on cloud height and cloud composition (liquid or ice); these properties differ between the winter and the summer. The overestimation of R_{in} in the winter and underestimation of R_{in} in the summer is one reason for why the MEM latent heat flux is biased high in the winter and biased low in the summer (Figures 3c and 3f). Developing separate ΔT parameterizations for warm and cold seasons may therefore improve these seasonal errors. The opposite MEM errors in the warm and the cold season explains why the mean bias in the annual λE is actually lower than the mean bias in the monthly λE (Table 1). These intermediate variables can suffer large errors and should not be used for other purposes except for computing λE in the MEM framework.

The mPT model (Equation 6) has the best performance among the three according to the performance matrix (Table 1). It is the recommended choice in situations where observational data on R_n is available. A natural question is whether the model with its parameter η tuned to the Lake Taihu observations ($\eta = 0.32$) can be extended to other lakes. To answer this question, in Figure 8 we compare the three parameterizations of β versus T_s against the lake evaporation data generated by a climate model for 1,400 lakes in the tropical and the temperate Köppen climate zones (K. Zhang et al., 2023). In the climate model, the lake-air fluxes of energy and water were computed at hourly time steps at the subgrid level using the Lake, Ice, Snow, and Sediment Simulator (Subin et al., 2012). The simulation year is 2016. The majority of these lakes (98.8%) are ice-free throughout the year. Each data point in Figure 8 represents a monthly value at one lake. This comparison shows that the tuned β parameterization is superior to the original PT or the oceanic parameterization.

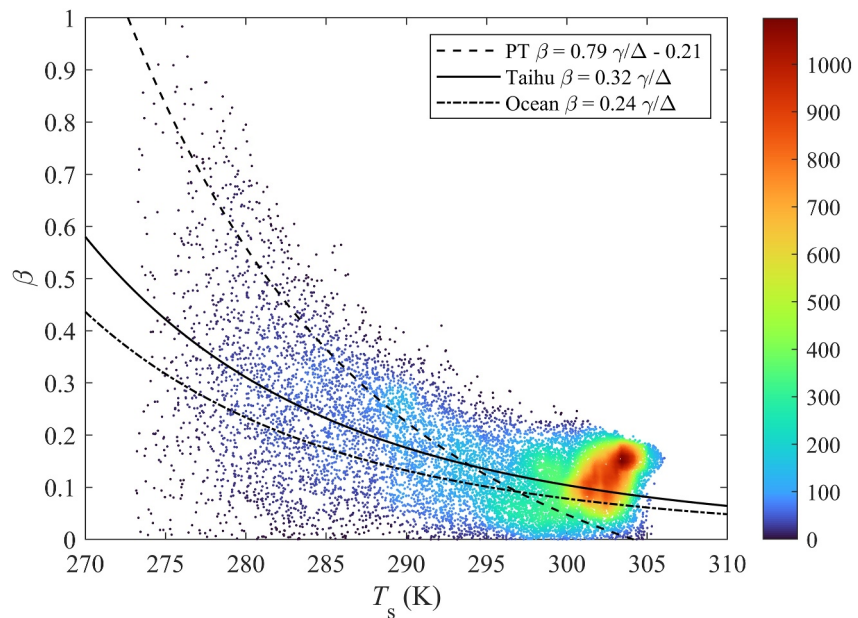


Figure 8. Comparison of three Bowen ratio parameterizations against the results of a global climate model simulation. Color indicates data density.

Parameter η in Figure 1 was obtained by minimizing the RMSE of β against the observed monthly β . Our values are within the range reported by Han and Guo (2023) for six water bodies in East Asia. We note that the tuned η is nearly identical for the large lake and the small fishpond, supporting the conclusion reached by Han and Guo (2023), that evaporation models based on energy conservation are independent of water body size.

Finally, all three models requires that the heat storage flux G be known. In the present study, G was determined with observations of water temperature profile (Wang et al., 2014). In situations where such observations are not available, G may be parameterized using the net radiation (Camuffo & Bernardi, 1982; Duan & Bastiaanssen, 2015) or an equilibrium temperature (de Bruin, 1982; G. Zhao & Gao, 2019). Future research should evaluate how these G parameterizations affect the performance of these models.

5. Conclusions

The results presented above support the use of locally-tuned relationship between Bowen ratio and the surface temperature and the coupling parameterization of the incoming and the outgoing longwave radiation. The PT model showed high biases in the latent heat flux in the warm season and low biases in the cold season; deployment of the tuned β - T_s relationship in the mPT model removed these biases. The MEM surface temperature was biased high in January by 9.7°C and only by 0.9°C in August. A consequence of this temperature bias is that the MEM net longwave radiation was biased high in the cold season and biased low in the warm season, which explains the high bias of the MEM latent heat flux in the cold season and low bias in the warm season. Another consequence is that the slope of the saturation vapor pressure function was too high in the cold season, which also contributed to the high bias of the MEM latent heat flux. When averaged over the observation periods, the MEM monthly mean bias error was 1.4 W m⁻² or 2% for the Lake and 2.4 W m⁻² or 3% for the fishpond and the annual mean bias error was 1.5 W m⁻² or 2% for the lake and 0.2 W m⁻² or 0.2% for the fishpond; these errors seem acceptable for most applications.

A key assumption of the MEM, that the incoming and the outgoing longwave radiation are fully coupled, is originally proposed for the extensive global ocean surface and for the monthly time interval. We found it to be a good approximation at both the annual and the month time scales and for the large lake as well as for the small fishpond. Reasons for why these two streams of longwave radiation should be coupled at time scales longer than a month and at such a small spatial scale are discussed. These results support the MEM as a practical alternative to the PT model at locations without net radiation measurement.

The mPT model that has incorporated a locally-tuned parameterization of the β dependence on temperature produces the best performance among the three models. Application of this model is contingent upon the availability of R_n observation. Comparison with a climate model simulation suggests that the β parameterization tuned to Lake Taihu observations be applicable to other lakes in temperate and tropical climates under ice-free conditions, but a firm conclusion will require evaluation against more lake observations.

Data Availability Statement

The observation data are available at (Xiao et al., 2024).

Acknowledgments

This research was supported by the National Natural Science Foundation of China (42021004, 41975143); the Natural Science Foundation of Jiangsu Province for Distinguished Young Scholars (BK20220055); the R&D Foundation of Jiangsu Province (BK20220020); and the 333 Project of Jiangsu Province (BRA2022023).

References

- Andreas, E. L., & Cash, B. A. (1996). A new formulation for the Bowen ratio over saturated surfaces. *Journal of Applied Meteorology*, 35(8), 1279–1289. [https://doi.org/10.1175/1520-0450\(1996\)035<1279:anftb>2.0.co;2](https://doi.org/10.1175/1520-0450(1996)035<1279:anftb>2.0.co;2)
- Campbell, G. S., & Norman, J. (2012). *An introduction to environmental biophysics*. Springer Science & Business Media.
- Camuffo, D., & Bernardi, A. (1982). An observational study of heat fluxes and their relationships with net radiation. *Boundary-Layer Meteorology*, 23(3), 359–368. <https://doi.org/10.1007/bf00121121>
- de Bruin, H. A. R. (1982). Temperature and energy balance of a water reservoir determined from standard weather data of a land station. *Journal of Hydrology*, 59(3–4), 261–274. [https://doi.org/10.1016/0022-1694\(82\)90091-9](https://doi.org/10.1016/0022-1694(82)90091-9)
- Downing, J. A., Prairie, Y. T., Cole, J. J., Duarte, C. M., Tranvik, L. J., Striegl, R. G., et al. (2006). The global abundance and size distribution of lakes, ponds, and impoundments. *Limnology & Oceanography*, 51(5), 2388–2397. <https://doi.org/10.1016/B978-012370626-3.00025-9>
- Duan, Z., & Bastiaanssen, W. G. M. (2015). A new empirical procedure for estimating intra-annual heat storage changes in lakes and reservoirs: Review and analysis of 22 lakes. *Remote Sensing of Environment*, 156, 143–156. <https://doi.org/10.1016/j.rse.2014.09.009>
- Fisher, J. B., Dohlen, M. B., Halverson, G. H., Collison, J. W., Pearson, C., & Huntington, J. L. (2023). Remotely sensed terrestrial open water evaporation. *Scientific Reports*, 13(1), 8174. <https://doi.org/10.1038/s41598-023-34921-2>
- Golub, M., Thiery, W., Marcé, R., Pierson, D., Vanderkelen, I., Mercado-Bettin, D., et al. (2022). A framework for ensemble modelling of climate change impacts on lakes worldwide: The ISIMIP lake sector. *Geoscientific Model Development*, 15(11), 4597–4623. <https://doi.org/10.5194/gmd-15-4597-2022>
- Han, S., & Guo, F. (2023). Evaporation from six water bodies of various sizes in East Asia: An analysis on size dependency. *Water Resources Research*, 59(6), e2022WR032650. <https://doi.org/10.1029/2022WR032650>
- Hicks, B. B., & Hess, G. D. (1977). On the Bowen ratio and surface temperature at sea. *Journal of Physical Oceanography*, 7(1), 141–145. [https://doi.org/10.1175/1520-0485\(1977\)007<0141:otbras>2.0.co;2](https://doi.org/10.1175/1520-0485(1977)007<0141:otbras>2.0.co;2)
- Lee, X. (2023). *Fundamental of boundary-layer meteorology* (2nd ed.). Springer.
- Lee, X., Liu, S., Xiao, W., Wang, W., Gao, Z., Cao, C., et al. (2014). The Taihu Eddy Flux Network: An observational program on energy, water and greenhouse gas fluxes of a large freshwater lake. *Bulletin of the American Meteorological Society*, 95(10), 1583–1594. <https://doi.org/10.1175/BAMS-D-13-00136.1>
- Liu, H., Blanken, P. D., Weidinger, T., Nordbo, A., & Vesala, T. (2011). Variability in cold front activities modulating cool-season evaporation from a southern inland water in the USA. *Environmental Research Letters*, 6(2), 024022. <https://doi.org/10.1088/1748-9326/6/2/024022>
- Liu, Z., Han, J., & Yang, H. (2022). Assessing the ability of potential evaporation models to capture the sensitivity to temperature. *Agricultural and Forest Meteorology*, 317, 108886. <https://doi.org/10.1016/j.agrformet.2022.108886>
- Liu, Z., & Yang, H. (2021). Estimation of water surface energy partitioning with a conceptual atmospheric boundary layer model. *Geophysical Research Letters*, 48(9), e2021GL092643. <https://doi.org/10.1029/2021GL092643>
- McGloin, R., McGowan, H., & McJannet, D. (2015). Effects of diurnal, intra-seasonal and seasonal climate variability on the energy balance of a small subtropical reservoir. *International Journal of Climatology*, 35(9), 2308–2325. <https://doi.org/10.1002/joc.4147>
- McMahon, T. A., Finlayson, B. L., & Peel, M. C. (2016). Historical developments of models for estimating evaporation using standard meteorological data. *Wiley Interdisciplinary Reviews- Water*, 3(6), 788–818. <https://doi.org/10.1002/wat2.1172>
- Penman, H. L. (1948). Natural evaporation from open water, bare soil and grass. *Proceedings of the Royal Society of London. Series A, Mathematical and Physical*, 193(1032), 120–145. <https://doi.org/10.1098/rspa.1948.0037>
- Priestley, C. H. B., & Taylor, R. J. (1972). On the assessment of surface heat flux and evaporation using large-scale parameters. *Monthly Weather Review*, 100(2), 81–92. [https://doi.org/10.1175/1520-0493\(1972\)100<0081:otaosh>2.3.co;2](https://doi.org/10.1175/1520-0493(1972)100<0081:otaosh>2.3.co;2)
- Raghuraman, S. P., Paynter, D., Menzel, R., & Ramaswamy, V. (2023). Forcing, cloud feedbacks, cloud masking, and internal variability in the cloud radiative effect satellite record. *Journal of Climate*, 36(12), 4151–4167. <https://doi.org/10.1175/jcli-d-22-0555.1>
- Stephens, G. L., & Hu, Y. (2010). Are climate-related changes to the character of global-mean precipitation predictable? *Environmental Research Letters*, 5(2), 025209. <https://doi.org/10.1088/1748-9326/5/2/025209>
- Stephens, G. L., Wild, M., Stackhouse, P. W., Jr., L'Ecuyer, T., Kato, S., & Henderson, D. S. (2012). The global character of the flux of downward longwave radiation. *Journal of Climate*, 25(7), 2329–2340. <https://doi.org/10.1175/JCLI-D-11-00262.1>
- Subin, Z. M., Riley, W. J., & Mironov, D. (2012). An improved lake model for climate simulations: Model structure, evaluation, and sensitivity analyses in CESM1. *Journal of Advances in Modeling Earth Systems*, 4(1), M02001. <https://doi.org/10.1029/2011MS000072>
- Tu, Z., & Yang, Y. (2022). On the estimation of potential evaporation under wet and dry conditions. *Water Resources Research*, 58(4), e2021WR031486. <https://doi.org/10.1029/2021WR031486>
- Tu, Z., Yang, Y., & Roderick, M. L. (2022). Testing a maximum evaporation theory over saturated land: Implications for potential evaporation estimation. *Hydrology and Earth System Sciences*, 26(7), 1745–1754. <https://doi.org/10.5194/hess-26-1745-2022>
- Verpoorter, C., Kutser, T., Seekell, D. A., & Tranvik, L. J. (2014). A global inventory of lakes based on high-resolution satellite imagery. *Geophysical Research Letters*, 41(18), 6396–6402. <https://doi.org/10.1002/2014GL060641>
- Wang, W., Chakraborty, T. C., Xiao, W., & Lee, X. (2021). Ocean surface energy balance allows a constraint on the sensitivity of precipitation to global warming. *Nature Communications*, 12(1), 2115. <https://doi.org/10.1038/s41467-021-22406-7>
- Wang, W., Lee, X., Xiao, W., Liu, S., Schultz, N., Wang, Y., et al. (2018). Global lake evaporation accelerated by changes in surface energy allocation in a warmer climate. *Nature Geoscience*, 11(6), 410–414. <https://doi.org/10.1038/s41561-018-0114-8>

- Wang, W., Xiao, W., Cao, C., Gao, Z., Hu, Z., Liu, S., et al. (2014). Temporal and spatial variations in radiation and energy balance across a large freshwater lake in China. *Journal of Hydrology*, *511*, 811–824. <https://doi.org/10.1016/j.jhydrol.2014.02.012>
- Xiao, W., Wang, J., Zhao, R., Jia, L., Chu, H., Bao, H., et al. (2024). Evaluation of the maximum evaporation and the Priestley-Taylor models for inland waterbodies [Dataset]. *Harvard Dataverse*, V3. <https://doi.org/10.7910/DVN/WW4RDS>
- Xiao, W., Zhang, Z., Wang, W., Zhang, M., Liu, Q., Hu, Y., et al. (2020). Radiation controls the interannual variability of evaporation of a subtropical Lake. *Journal of Geophysical Research: Atmospheres*, *125*(8), e2019JD031264. <https://doi.org/10.1029/2019JD031264>
- Yang, Y., & Roderick, M. L. (2019). Radiation, surface temperature and evaporation over wet surfaces. *Quarterly Journal of the Royal Meteorological Society*, *145*(720), 1118–1129. <https://doi.org/10.1002/qj.3481>
- Yao, Y., Liang, S., Li, X., Chen, J., Wang, K., Jia, K., et al. (2015). A satellite-based hybrid algorithm to determine the Priestley-Taylor parameter for global terrestrial latent heat flux estimation across multiple biomes. *Remote Sensing of Environment*, *165*, 216–233. <https://doi.org/10.1016/j.rse.2015.05.013>
- Yu, L., & Weller, R. A. (2007). Objectively analyzed air-sea heat fluxes for the global ice-free oceans (1981-2005). *Bulletin of the American Meteorological Society*, *88*(4), 527–539. <https://doi.org/10.1175/BAMS-88-4-527>
- Zhang, K., Lee, X., Schultz, N. M., Zhao, L., He, C., Huang, Q., et al. (2023). A global dataset on subgrid land surface climate (2015-2100) from the Community Earth System Model. *Geoscience Data Journal*, *10*(2), 208–219. <https://doi.org/10.1002/gdj3.153>
- Zhang, Z., Zhang, M., Cao, C., Wang, W., Xiao, W., Xie, C., et al. (2020). A dataset of microclimate and radiation and energy fluxes from the Lake Taihu eddy flux network. *Earth System Science Data*, *12*(4), 2635–2645. <https://doi.org/10.5194/essd-12-2635-2020>
- Zhao, G., & Gao, H. (2019). Estimating reservoir evaporation losses for the United States: Fusing remote sensing and modeling approaches. *Remote Sensing of Environment*, *226*, 109–124. <https://doi.org/10.1016/j.rse.2019.03.015>
- Zhao, J., Zhang, M., Xiao, W., Jia, L., Zhang, X., Wang, J., et al. (2021). Large methane emission from freshwater aquaculture ponds revealed by long-term eddy covariance observation. *Agricultural and Forest Meteorology*, *308–309*, 108600. <https://doi.org/10.1016/j.agrformet.2021.108600>
- Zhao, J., Zhang, M., Xiao, W., Wang, W., Zhang, Z., Yu, Z., et al. (2019). An evaluation of the flux-gradient and the eddy covariance method to measure CH₄, CO₂, and H₂O fluxes from small ponds. *Agricultural and Forest Meteorology*, *275*, 255–264. <https://doi.org/10.1016/j.agrformet.2019.05.032>